

Improvement of Corrosion and Sliding Wear Behavior of Tin-Bronze Alloys Reinforced by ZrO₂ Particles Prepared via Powder Technology

Khalid Mutashar Abed

College of Materials Engineering- Metallurgical Engineering department, Babylon University.

Nawal Mohammed Dawood*

College of Materials Engineering- Metallurgical Engineering department, Babylon University.

*corresponding author: Nawal Mohammed Dawood

Abstract

Powder metallurgy was used to generate samples of an alloy consists of tin-bronze with a chemical composition of 90% Cu and 10% Sn in the current study. To generate the samples in addition to the base alloy, zirconia (3 percent, 6 percent, and 9 wt. percent) was added to the original alloy to evaluate the additives influence on corrosion, mechanical, physical, and sliding wear behavior. The powders were blended for 6 hours before being pressed at 600 MPa. The prepared samples were sintered at 200°C for one hour, then increased to 600°C for three hours at a rate of 10°C/min in a vacuum atmosphere (10⁻⁴ torr), then allowed to cool inside the furnace until room temperature while maintaining continuous air discharge. Using the Tafel extrapolation technique, all samples were evaluated to investigate corrosion behavior. Further wear behavior was investigated utilizing the Ball-on-Disc approach, with several constants of wear factors such as applied force and rotational speed, during a 25-minute period. The influence of ZrO₂ micro particles on the topography of surfaces was investigated using a scanning electron microscope. The reinforced alloy microstructure is constituted of a fine dendritic structure of Cu phase and Cu₃Sn as an intermetallic compound, according to the findings. In a 3.5 percent NaCl solution at ambient temperature, the samples reinforced with 9wt% ZrO₂ have a lower corrosion rate (11.573 mpy) than other composite materials. When 9 wt. ZrO₂ micro-particles are added to the alloy, the wear rate drops to (0.3987x10⁻⁸ g/mm) at the optimum conditions of 20 N, 300 rpm, and 25 minutes. The microstructure of the worm surface revealed that delamination is reduced as a result of improving alloy wear resistance and hardness through micro particle reinforcement.

Keywords: Powder metallurgy, Tin bronze alloy, Porous structures, wet sliding wear Behavior, Corrosion behavior.

I. Introduction

Copper and copper alloys are one of the main groups of commercial metals. Fine art products cast from copper alloys always be interested from the past until now. Right from the bronze age, humans started to know manipulated labor tools, weapons, currency, jewelry, musical instruments, and then to the monument carries historical significance for daily activities service and traditional culture needs to resume, remind people to remember the thanks of generations go-ahead has been achieved in the development process society. Copper and copper alloys have been minted since 2000 BC. The archaeologists estimate that from 7000 BCE bronze has been wrought and rolled, and from 5000 BC bronze was melted and poured into molds made of stone and pottery. From there, the ancient people have discovered that if copper is mixed with arsenic metals then alloys became more rigid and more ductile. After that, arsenic was replaced with tin, and bronze was discovered; bronze consists of about 80% copper, 1 ~ 2% tin, and zinc, the rest consists of many small amounts with elements, including lead [1].

Because of their outstanding thermal and electrical conductivity, as well as their ease of fabrication and corrosion resistance, Cu-based alloys, such as bronzes sought after for industry such as railway application, contact wires, connectors, lead frames, pipes, radiators, heat exchangers, and valves [2, 3]. The corrosion of copper is usually an electrochemical reaction in which the metal melts as ions at anodic sites and hydrogen from the electrolyte is deposited at the cathodic area. Copper, as a noble metal, does not generally displace hydrogen ions from a solution containing them [4]. Copper corrosion is thought to involve a concurrent dissolution of anodic and cathodic oxygen reduction process [5], as well as a chemical reaction involving an oxygen molecule [6]. Anderson et al [7] reported an increase in copper corrosion rate due to increased chemical interaction between cuprous ions and

oxygen, i.e.:



A chemical redox between cuprous intermediate Cu (I) ads and oxygen reduction reaction intermediate (HOx) ads synergistically, rather than an oxygen molecule, was previously attributed to a cathodic electrochemical oxygen reduction reaction acceleration at the corrosion potential [8]. Milan et.al describes the anodic breakdown of copper in acidic media [9]:



The corrosion reaction at the cathode in an aerated acidic solution is a process of oxygen reduction expressed in the following [10]:



Due to its good ability for casting, high resistance against corrosion, high aesthetic value, and low porosity, bronze (a Cu–Sn alloy) is frequently employed in manufacturing of some materials used for electrical applications,[11] ion battery industries,[12,13], archeological artifacts and casting [14,15]. Patina, a passivation layer, accumulates on the bronze alloys surface over time. Patina on artworks and archeological items is frequently thought to have an aesthetic value. It also serves as a protective layer and is relatively stable. Robbiola et al. established two kinds of patina development methods (Type I and Type II), used to clarify corrosion layers that formed on alloys of Cu–Sn. [16, 17]. In the introduction of sulfate ions, Type I typically forms a two layer structure. It involves the growth of a thin Sn-rich layer immediately on the basic alloy surface, as well as selective dissolution of Cu. Cu ions move from the surface of the alloy to the outer surface via the corrosion layer rich by Sn, where they either form insoluble Cu complexes with the anions or dissolve in the corrosive media. In the case of the Type II mechanism, its structure is characterized by a characteristic 3-layer thick patina that resembles to environments comprising chlorides or the existence of heterogeneities in the alloy. Corrosion can be localized or widespread, and it develops at the bulk alloy expense, perhaps leading to the alloy's full breakdown.

Many studies have studied the wear properties of copper-based self-lubricated composites [18-24]. The wear resistance and friction coefficient of MMCs are affected by load, material composition, hardness, lubrication surface, treatments, according to research on Al-40Zn-3Cu2Si alloy and SAE 65 bronze [25]. Dhokey and Paretkar [26] investigated the wear mechanism of copper-based SiC composites in terms of mechanical and thermal characteristics for various speeds and loads, and used a dimensional technique to show the mild and severe wear regimes. To improve the wear and friction properties of sintered materials, many solid lubricants were added. The sliding properties of Cu-Sn-based composite materials comprising WS2 and graphite at high speeds were outstanding [23]. The inclusion of graphite to C-SiC composites was investigated to improve their wear properties [22, 27].The goal of this study is to use a potentiostat polarization at dry sliding condition on a Ball-on-Disc tribometer (BODT) to evaluate the corrosion resistance of Tin bronze alloy (Cu-10 wt. percent Sn) strengthened by ZrO₂ micro particles in 3.5 percent NaCl solution.

2. Experimental Work

2.1. Sample Preparation

The powder metallurgy method (PMM) was utilized to manufacture the samples in this investigation, and the metal powders employed (Copper, Tin, and Zirconia) are listed in Table 1 along with their purity, particle size, and provenance.

Table 1: Average Size of the particle and purity of the Powder.

powder	Purity%	Averageparticle size(µm)	Company or supplier
Cu	99.99	19.90	BDH Chemicals Ltd / England
Sn	99.87	15.64	BDH Chemicals Ltd / England
ZrO ₂	99.95	10.90	BDH Chemicals Ltd / England

2.1.1 Preparation of powder

To decrease oxidation and friction in the powder particles caused by the mixing process, wet mixing was performed in the introduction of (2 wt.%) Ethyl alcohol. As indicated in Table 2, a base alloy (B) was made using a mixture of (90 wt. percent Cu-10 wt. percent Sn) with varied quantities of ZrO₂ (3, 6, and 9 wt. percent) to prepare composite alloys (B1, B2, B3). To produce the correct and homogenous dispersion of powder particles, the mixing procedure was carried out for 5 hours in a ball mill type (STGQM-15/-2). The mixture was dried for 30 minutes at 60 degrees Celsius.

2.1.2.Compaction of Powder

Cylindrical one-direction action dies were utilized to prepare the samples. The disk-shaped samples were manufactured with 13 mm and 8 mm for diameter and height, respectively. A stress of 600 MPa is applied on the metallic powders in order to obtain green compacting samples using a one-channel electrical-hydraulic press of type CT340-CT440. All compacting processes lasted 8 minutes and were carried out at a constant rate of loading (0.3) KN/sec. To obtain the desired pressure, graphite was used to grease the interior walls of the steel die.

Table 2: Prepared Samples.

Samples code	Sn wt. %	ZrO ₂ wt. %	Cu wt. %
Base alloy (B)	10	0	Bal.
B 1	10	3	Bal.
B 2	10	6	Bal.
B 3	10	9	Bal.

2.3. Sintering Process

The green compacts sintering was done in a vacuum tube furnace (MTI-1) under vacuum conditions (GSL1600X). The pressure was set at 10⁻⁴ torr. As illustrated in Figure 1, the sintering procedure for the samples involved the following steps:

- Heat to (200°C) from room temperature and soak for (60) minutes within a rate of (10°C/min).
- Heat from 200°C to 600°C and soak for 180 minutes at a rate of 10°C/min.
- Slowly cool the furnace to ambient temperature while maintaining the suction.

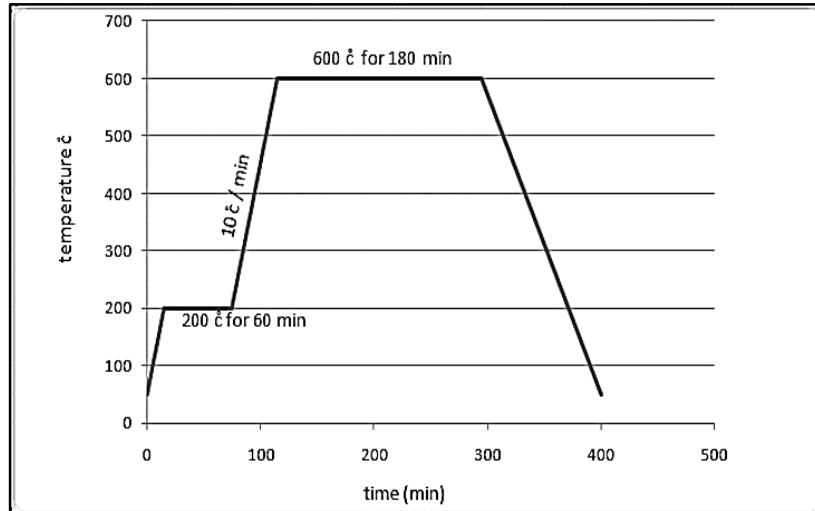


Figure 1: The Green Samples Sintering Program.

3. Testes of Samples

3.1. Scanning Electron Microscopy (SEM) and (EDS) Analysis

Sintered samples were ground to 400, 800, 1200, and 2000 grits on SiC paper before being polished with diamond solution. The samples were etched at room temperature using (5g FeCl₃ + 3 ml HCl + 92 ml distilled water) [28]. Following etching, the samples were rinsed with distilled water and dried with an electric drier. SEM images were taken in order to examine the microstructure with high precision, define the surface form, porosity, and pore size along with the examination of the chemical composition (EDS).

3.2. Density and Porosity Testing

Sintered samples were tested for density and porosity according to ASTM B-328 [29]:

- ❖ The sample was weighted after drying for 5 hours at 100°C in a vacuumed furnace under (10⁻⁴ torr), and the weight represented mass (A).
 - ❖ The sample is totally immersed in dense oil of (0.8 g/cm³) for 30 minutes at room temperature.
 - ❖ To get the mass B, weigh the totally saturated sample in air. To get the mass C, weigh the fully resulted sample in water.
- The following equations [30] were used to compute density and porosity:

$$P = \left[\frac{B-C}{D_o(B-c)} \right] \times 100 \quad D_w \dots \dots \dots 5$$

$$D = \left[\frac{A}{D_o(B-c)} \right] D_w \dots \dots \dots 6$$

Where:

- D_o = oil density (0.8 g/cm³)
- D_w = water density (1 g/cm³)

3.3. Micro-Hardness Examination

This test was performed according to ASTM E384 using a Vickers micro hardness device (digital micro Vickers hardness tester TH 717) and a load of (300g) lasting for (10sec). The results were recorded as an average of six readings for each prepared

sample.

3.4. Polarization Experiments

The cathodic and anodic behaviors, or corrosion reactions monitoring on desired metal samples, are observed using the polarization approach for corrosion behavior. According to the ASTM, electrochemical tests were conducted using a potentiostatic type (winking M lab 200, Germany) (ASTM). The corrosion test samples are machinated to a 13 mm in diameter and 4 mm in thickness. The electrochemical cell is made up of a 1000 ml container filled with a 3.5 percent NaCl solution that is used to submerge the three electrodes. A reference, working, and counters (auxiliary) electrodes make up the electrochemical cell. The reference electrode is the Calomel Standard Electrode (saturated calomel electrode) [30]. The materials that need to be evaluated are related to the working electrode. As a counter electrode, a platinum rod (100 mm x 10 mm) is employed. The electrode is responsible for carrying the current in the circuit. As indicated in Figure 2, the counter electrode that used for measuring the voltage between the W.E. and the electrolyte is respected by the reference electrode. The electrodes were connected using a potentiostat (M Lab 200, Germany), and the experiments were conducted at room temperature with a 2 mV/s scanning rate within the prepared solution. Equation 7 is used to determine the corrosion rate during the electrochemical reaction with respect to the current density in the solution [31]: -

$$CR \text{ (mpy)} = 0.13 \times icorr \ e / \rho \dots\dots\dots 7$$

Where: CR: Corrosion rate (mpy) ,
 icorr: current density of corrosion ($\mu\text{A}/\text{cm}^2$).
 e : Equivalent weight (atomic weight / valance).
 ρ: Metal density (g/cm^3).

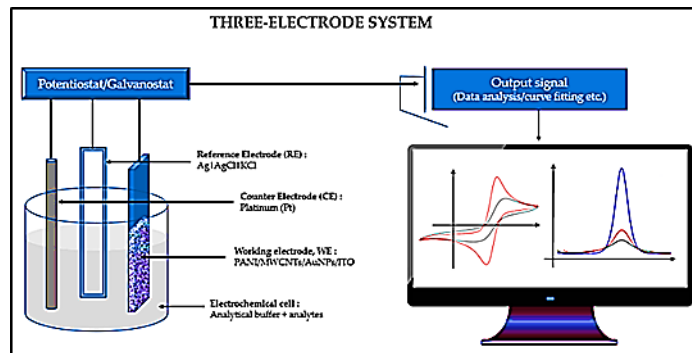


Figure 2. A Computer-controlled potentiostatic/galvanostat with a standard three-electrode system connected to an electrochemical cell [32]

3.4. Sliding Wear Test

In compliance with ASTM G99, dry sliding wear was tested utilizing (BOD) Micro Test Wear-Madrid Spain using steel balls made of 100 Cr6 martensitic bearing of steel with a constant value of the radius of (5mm). The test lasted 25 minutes and covered a distance of 100 meters, as illustrated in Figure 3. These tests were carried out at constant speed and load of 400 rpm and 20 N, respectively. The wear resistance have been determined. The following equation [34] calculates the wear rate:

$$\text{Wear Rate (WR)} = \Delta W / \pi D N t \dots\dots\dots 8$$

Where : ΔW : Weight loss for the test (g) ,
 D: sliding circle diameter (0.5 cm),
 t: time of the wear test (20min)
 N: Disc rotational speed (rpm)

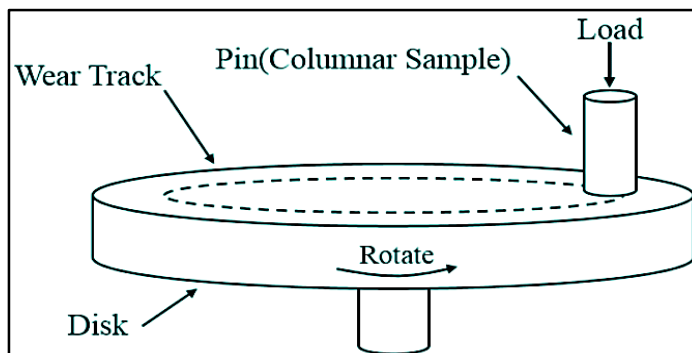


Figure 3. Schematic diagram of a pin-on-disk wear test set-up [33].

4. Results and Discussion.

4.1. Microscope and X-Ray Diffraction Analysis

The microstructure has a substantial impact on all properties of the tin-bronze alloy. So, after examining the microstructure of four alloys (B, B1, B2, and B3) with (SEM), it was discovered that alloy (B) had a dark region microstructure representing α (Cu, Sn)-phase as the alloy matrix and bright region of (Cu_3Sn) as intermetallic resulted compound, whereas samples B1, B2, and B3 had a dark microstructural region representing α (Cu, Sn) phase, bright region of (ϵ - Cu_3Sn). The particles of ZrO_2 depicted in Figures 4 are denoted by red arrows. The (XRD) pattern for a base alloy is shown in Figure 5. The results of XRD of the alloys show the existence of two phases: α (Cu, Sn)-phase as the alloy's matrix and ϵ - (Cu_3Sn) as the intermetallic phase, which agrees with [35].

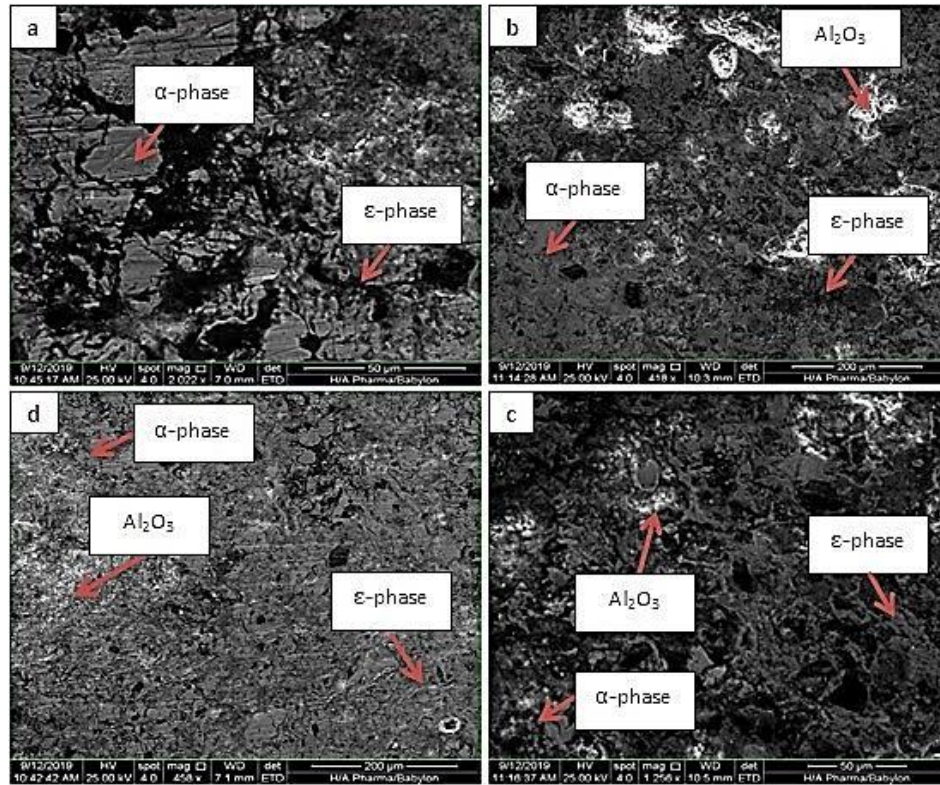


Figure 4: SEM-Image represents Morphology of (a) Base alloy (B), (b) B1, (c) B2, and (d) B3 alloys

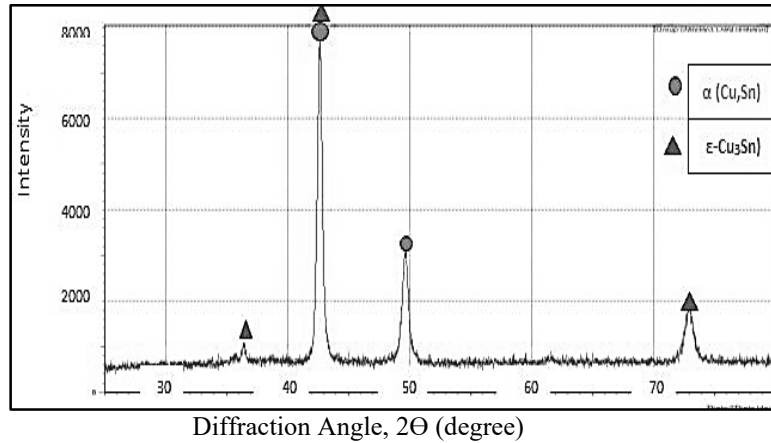


Figure 5: XRD Pattern Analysis for Base Alloy (B).

4.2. Density and Porosity Results

The experimental porosity and density values for alloys are shown in Figures 6 and 7, respectively for the alloys (B, B 1, B 2 and B3). As can be observed, the densities of the alloys (B1, B2, and B3) are lower than those of the base alloy (B), while the porosity is higher. This is due to the addition of Zirconium oxide, which has a lower density value than copper and tin, reduced the amount of copper and tin. Zirconium oxide has a density of 5.68 g/cm³, whereas copper and tin have densities of (8.9 g/cm³) and (7.3 g/cm³), respectively. In contrast, the particle size of zirconium oxide is (10.90 μm) which tend to reduce the pores between the copper and tin particles during the compacting process, as the particle size of the copper and tin are 19.9 μm, 15.64 μm, respectively, which led to a decrease in the porosity with an increase in the content of zirconium oxide [36].

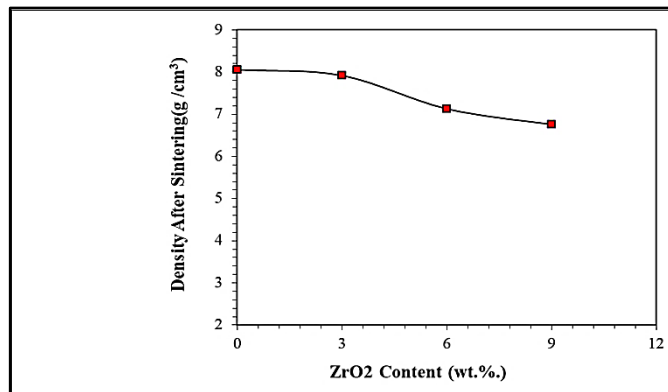


Figure 6: Density of Prepared Alloys vs. ZrO₂ content (wt.%)

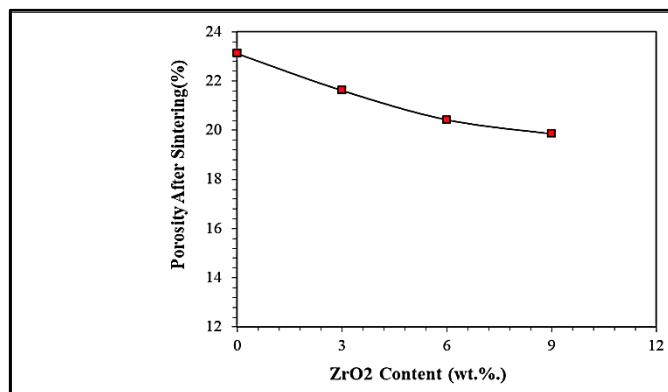


Figure 7: Porosity of Prepared Alloys vs. ZrO₂ content (wt.%)

4.3. Hardness Results

Figure 8 depicts the hardness of the investigated materials. The microstructure, kind of material, and alloying components all influence a material's hardness. Because dislocation motion causes plastic deformation in crystals, any impediment to dislocation

motion will prevent deformation, resulting in grain strengthening [37]. As can be seen, the addition of (ZrO₂) particles results in an increase in hardness because of the strengthening, which induced by (ZrO₂) particles. The matrix passes part of the particles induced applied stress, which stand a percentage of the load, and these particles try to constrain matrix phase movement in the region of each particle. The involvement of these particles as impediment dislocation motion causes the strengthening effect. These particles establish an incoherent contact with the matrix, causing a large dislocations number to develop at the interface, strengthening the material [38].

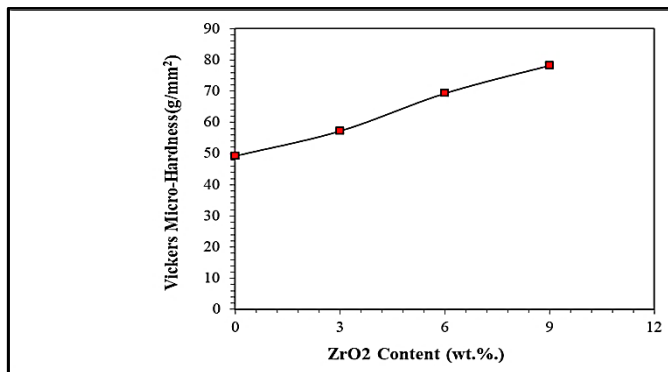


Figure 8: Vickers Hardness of Prepared Alloys vs. ZrO₂ content (wt.%)

4.4. Corrosion Test

In the test of the electro-chemical corrosion of all samples with a pH of 7.4, the Tafel extrapolation method was applied. Using this method, the parameters of corrosion, E_{corr} and i_{corr} were calculated. i_{corr} and E_{corr} represent the interaction of these two curves of polarization. As shown in Figure 9a, the i_{corr} and E_{corr} values for Cu-10 wt% Sn alloy without micro particles are 73.21 A/cm² and - 313 mV, respectively. As shown in Figure 9d, the corrosion resistance characteristics, i_{corr} (17.82 A/cm²) and E_{corr} (- 97 mV), improve when the sample is manufactured and reinforced with micro particles (9 wt. percent ZrO₂). Table 3 demonstrates that with the addition of micro particles of ZrO₂, the corrosion rate of samples dropped from 40.448 mpy to 11.573 mpy, owing to increased passive behavior of micro particles added at 9 wt. percent ZrO₂.

Table 3. Shows that corrosion parameters of the Cu-Sn reinforced by ZrO₂ micro particles.

Samples code	Icorr $\mu\text{A}/\text{cm}^2$	E mV	Corrosion rate mpy	Improvement Percentage
Base alloy (B)	73.21	- 313	40.448
B 1	39.80	- 306	27.255	32.61
B 2	30.98	-318	17.331	57.15
B 3	17.82	- 97	11.573	71.38

The presence of micro particles ZrO₂ in the matrix caused a decrease in corrosion current density. This is because micro particles strengthen the durability of coatings oxide of surface generated on the surface of the material. The behavior of polarization of Cu alloys in solutions of the chloride appears to be dominated by copper dissolution to cuprous solubility as complex chloride ion CuCl. The diffusion rate of CuCl ions from the surface of the electrode through the diffusion layer controls it. Corrosion behavior varies due to differences in microstructure.

4.5. Wear Rate

The effect of various ZrO₂ micro particle additions on the rate of wear under dry sliding conditions has been examined. The rotational speed, load, and time were all set at 300 rpm, 20 N, and 25 minutes, respectively. Due to microscopic nature of Cu-Sn being containing single phase (α) [39] and soft nature, it has a high wear rate of 1.393310^{-8} g/mm when compared to other alloys (Figure 10). When 9 wt% ZrO₂ micro particles are added to the alloy, the wear rate drops to $(0.396710^{-8}$ g/mm). This means that adding the tiny particles improves the alloy's wear resistance significantly.

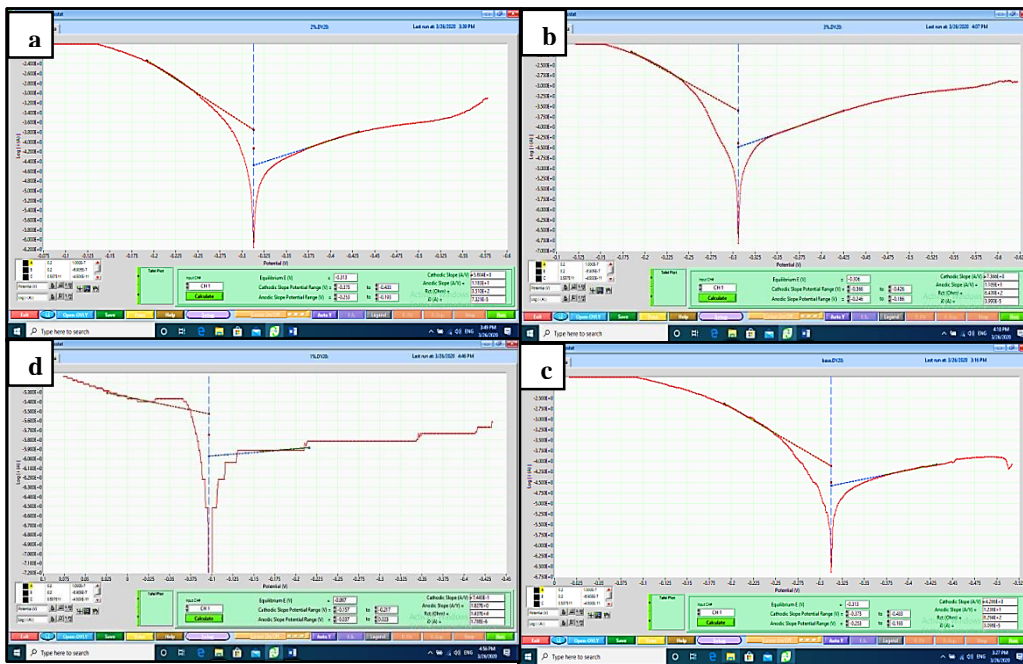


Figure 9. Shows the polarization curves of (a) Base alloy (B) , (b) B 1 . (c) B 2 ,and (d) B 3 alloys

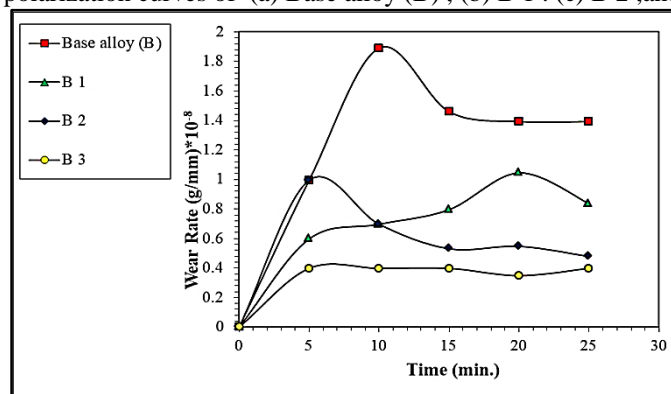


Figure 10: Wear rate for all samples at load 20 N.

This is thought to be owing to the tiny particles that cause the hardness to rise. As a result, the plastic deformation between the surfaces of contact is reduced, and the contact surfaces operate as a load-bearing element [40]. It has been shown that when the micro particles percentage increases, the wear rate of alloys decreases. Cu-Sn with micro ZrO_2 particles has a lower wear rate than matrix. This is because the tiny particles that increases the hardness of these alloys.

The Optical Microscope (OM) was used to examine the effect of micro particles of ZrO_2 on the topography of samples worn surfaces . This research was carried out under ideal conditions of 20 N, 300 rpm, and 25 min for force, rotating speed, and a time, respectively, with varying weight percentages on micro particles. The Cu-Sn alloy matrix worn surface is found to be more damaged on the worn surface, representing that the Cu-Sn alloy has undergone extensive plastic deformation and high disruption. Furthermore, among the strengthened alloys, there is a high wear rate and weight loss. The major wear mechanism of Cu-Sn alloy is adhesive wear generated by sliding surfaces. As seen in Figure 11, this causes substantial plastic deformation of subsurface and surface alloys under stress (a, b and c). Work hardening for unreinforced alloy of Cu-Sn happened after deformation, resulting in the emergence of microcracks. Figure 11 (a) shows how delamination happens in a Cu-Sn alloy with 3 wt% ZrO_2 when a small void forms, expands, and converges micro-cracks on the surface and subsurface.

Furthermore, it was discovered that tiny grooves constructed along the sliding direction, resulting in abrasive wear. Under wear circumstances, the phases reinforcement are characterized by the delamination mechanism, in which the hard reinforced particles break, fragment, and are partially or completely removed from the matrix phase [41]. The number of delamination layers and the depth of the grooves in the matrix are significantly higher in the matrix than in the reinforced alloy. Figure 11 (b to d) depicts the surface morphologies of samples after adding 3, 6, and 9 wt% ZrO_2 micro particles separately and collectively. Micro particles generate abrasive grooves, which prevent matrix delamination and chips separation the from the surface, as noticed in Figure 11. (b to d). As seen in Figure 11, the surface has some evident of the abrasive grooves in the longitudinal direction owing to the effects of hardness (b and d). Abrasion and plastic deformation are prevented by these hard particles, as seen in Figure 11. (b to d). This is owing to concentration of the stress on the contact surface and matrix-reinforcement bonding. The use of micro particles to strengthen alloys improves their wear resistance and increases their hardness, resulting in a reduction in delamination

[42].

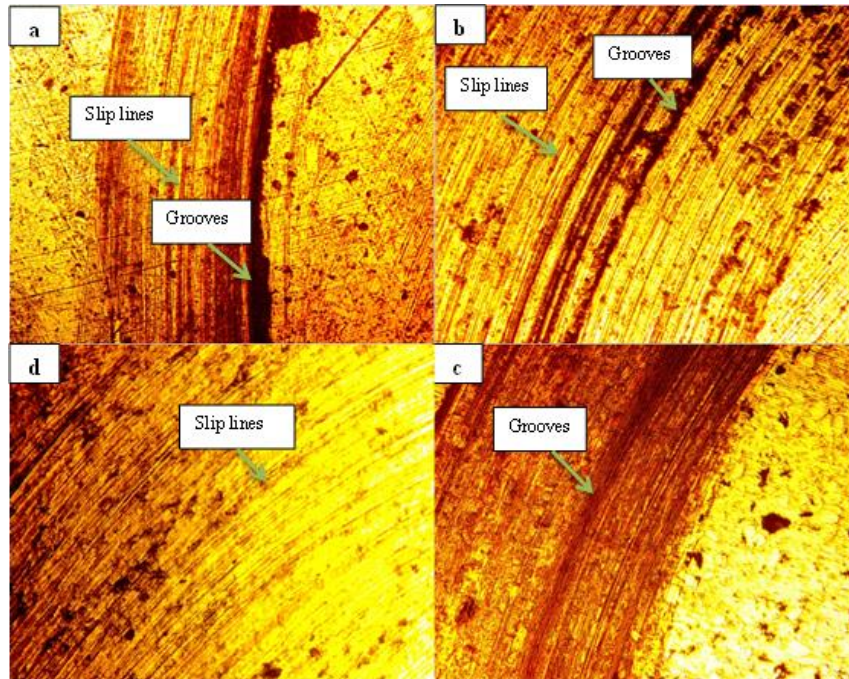


Figure 11. Shows the worn surface morphologies at load of 20 N and 300 rpm for all samples

5. Conclusions

1. The microstructure of the sample (A) (90 percent Cu, 10% Sn) obtained under the conditions of [(600) MPa, (600 °C), and (180) min for compacting pressure, sinter temperature, and period, respectively] consists of two phases: α (Cu, Sn) phase as the alloy matrix and (ϵ -Cu₃Sn) phase as the intermetallic phase.
2. The density of samples (B2, B3, and B4) is (7.92, 7.13, and 6.76 g/cm³, respectively, which is smaller than the base alloy (B) (8.06 g/cm³), and the samples porosity (B2, B3, and B4) is (21.62, 20.43, and 19.86 percent, respectively, which is lower than the base alloy (B) (23.12 percent)
3. It was discovered that the reinforced alloys corrode at a lesser rate in a 3.5 percent of the NaCl solution at room temperature with a pH of 7.4 than the unreinforced alloys.
4. When associated to the Cu Sn matrix, reinforced alloys with 3, 6, and 9 wt% ZrO₂ had a lower corrosion rate.
5. When ZrO₂ micro particles are added to Cu-Sn alloy, the Vickers microhardness value rises to 78.24 HV, compared to Cu Sn alloy's 49.23 HV.
6. Under the best conditions of 20 N, 300 rpm, and 25 min, the Cu-Sn alloy reinforced with 9wt% ZrO₂ has a lower wear rate (0.3987 X 10⁻⁸ g/ mm) than the matrix(1.3933 X 10⁻⁸ g/ mm) .
7. Abrasive and Adhesive mechanisms have been experiential in all alloys of Cu-Sn that treated by micro particles in the dry sliding wear.

6. References

- [1] Bui Binh Ha, Nguyen Hong Hai, Pham Mai Khanh, Corrosion Behavior and Castability of Different Bronze Alloys for Outdoor Sculptures, The 13th Asian Foundry Congress (AFC – 13), Hanoi, 2015.
- [2] Penga L and Xie H Effect of Heat Treatment on the Microstructure of Cu-Cr-Zr Alloy Key Engineering Materials 727, 2016,pp. 166-170.
- [3] Davis J R , Handbook Copper and Copper Alloys, Associates ASM Specialty 5 ,2001,pp. 113 -130
- [4] Walaa A. Hussein , Amal S. I. Ahmed , Wafaa A. Ghanem , Ghalia A. Gaber, Studies of Corrosion and Electrochemical Behavior of Cu-Zn Alloys in H₂SO₄ and HNO₃ Acid Solutions, Journal of Metallurgical Engineering (ME) Volume 5, 2016.
- [5] Pengju Liu, Xia Fang, Yongming Tang, Chunming Sun, Cheng Yao, Electrochemical and Quantum Chemical Studies of 5-Substituted Tetrazoles as Corrosion Inhibitors for Copper in Aerated 0.5 M H₂SO₄ Solution, Materials Sciences and Applications > Vol.2 No.9, September 2011.
- [6] Yonghong Lu, Wei Wang , Haibo Xu, Xiangfeng Kong , Jia Wang, Copper corrosion and anodic electrodisolution mechanisms in naturally aerated stagnant 0.5 M H₂SO₄, Volume 52, Issue 3, March 2010, pp.780-787
- [7] T. N. Andersen, M. H. Ghandehari and H. Eyring . A Limitation to the Mixed Potential Concept of Metal Corrosion: Copper in Oxygenated Sulfuric Acid Solutions, Journal of The Electrochemical Society, Volume 122, Number 12, 1975. pp. 1589-1595.

- [8] J. Porcayo-Calderon, R. A. Rodriguez-Diaz, E. Porcayo-Palafox, J. Colin, A. Molina-Ocampo, and L. Martinez-Gomez, Effect of Cu Addition on the Electrochemical Corrosion Performance of Ni₃Al in 1.0 M H₂SO₄, *Advances in Materials Science and Engineering* Volume 2015, Article ID 209286, 18 pages <http://dx.doi.org/10.1155/2015/209286>
- [9] Milan B. Radovanović, Žaklina Z. Tasić, Marija B. Petrović Mihajlović, Ana T. Simonović & Milan M. Antonijević, Electrochemical and DFT studies of brass corrosion inhibition in 3% NaCl in the presence of environmentally friendly compounds, *Scientific Reports*, 9, Article number: 16081, 2019.
- [10] Dahyun Choi, Suhee Kang, Hyungsub Kim, Hyojun Kim, and Caroline Sunyong Lee, Rapid Formation of Kinetically Sprayed Cu-Sn Intermetallic Film, *Hindawi, Journal of Nanomaterials*, Volume 2019, Article ID 4575079, 2019, p.6.
- [11] Ye, Bora; Kim, Sunjung, Formation of Nanocrystalline Surface of Cu-Sn Alloy Foam Electrochemically Produced for Li-Ion Battery Electrode, *Journal of Nanoscience and Nanotechnology*, Volume 15, Number 10, October 2015, pp. 8217-8221(5), <https://doi.org/10.1166/jnn.2015.11434>
- [12] Zhipeng Liang, Kaixi Jiang, Tingan Zhang, and Zhihe Dou, Corrosion behavior of Cu-Sn bronze alloys in simulated archeological soil media, *Materials and Corrosion*, 2019, pp. 1-11. DOI: 10.1002/maco.201911338
- [13] Michél Hauer, Frank Gärtner, Sebastian Krebs, Thomas Klassen, Makoto Watanabe, Seiji Kuroda, Werner, Process Selection for the Fabrication of Cavitation Erosion-Resistant Bronze Coatings by Thermal and Kinetic Spraying in Maritime Applications, *Journal of Thermal Spray Technology* volume 30, 2021, pp.1310-1328.
- [14] Liliana Gianni, Mauro Cavallini, Stefano Natali and Annemie Adriaens, Wet and Dry Accelerated Aging Tests in a Spray Chamber to Understand the Effects of Acid Rain Frequencies on Bronze Corrosion *Int. J. Electrochem. Sci.*, 8, 2013, pp. 1822 - 1838
- [15] Aymen Chaabani, Safa Aouadi, Nébil Souissi, X. Ramón Nóvoa, Electro-Chemical Impedance Spectral (EIS) Study of Patinated Bronze Corrosion in Sulfate Media: Experimental Design Approach, *Journal of Materials Science and Chemical Engineering*, Vol.5 No.10, October 31, 2017.
- [16] Robbiola, L, Blengino, J.M. and Fiaud, C. Morphology and Mechanisms of Formation of Natural Patinas on Archaeological Cu-Sn Alloys. *Corrosion Science*, 40, 1998, pp.2083-2111.
- [17] Luc Robbiola, Christian Fiaud, Contribution of statistical analysis of corrosion products to the understanding of the degradation processes of archaeological bronzes, *Archeosciences, revue d'Archéométrie*, G.M.P.C.A./Presses universitaires de Rennes, 1992, 16, pp.109-119. hal-00540407.
- [18] Ravindran, P., Manisekar, K., Narayanasamy, P., Selvakumar, N., and Narayanasamy, R., "Application of Factorial Techniques to Study the Wear of Al Hybrid Composites, with Graphite Addition," *Materials and Design*, 39, 2012, pp 42-54.
- [19] Tjong, S. C. and Ma, Z. Y., "Microstructural and Mechanical Characteristics of Composites," *Materials Science and Engineering*, 29, 2000, pp 49-113.
- [20] Kato, H., Takama, M., Iwai, Y., Washida, K., and Sasaki, Y., "Wear and Mechanical Properties of Sintered Copper-Tin Composites Containing Graphite or Molybdenum Disulfide," *Wear*, 255, 2003, pp 573-578.
- [21] Tsuya, Y., Shimura, H., and Umeda, K., "A Study of the Properties of Copper and Copper-Tin Base Self Lubricating Composites," *Wear*, 22, 1972, pp 143-162.
- [22] Ramesh, C. S., Noor Ahmed, R., Mujeebu, M. A., Abdullah, M. Z., "Development and Performance Analysis of Novel Cast Copper-SiC-Gr Hybrid Composites," *Materials and Design*, 30, 2009, pp 1957-1965.
- [23] Watanabe, Y., "High-Speed Sliding Characteristics of Cu-Sn-Based Composite Materials Containing Lamellar Solid Lubricants by Contact Resistance Studies," *Wear*, 264, 2008, pp 624-631.
- [24] Moustafa, S. F., El-Badry, S. A., Sanad, A. M., Kieback, B., "Friction and Wear of Copper-Graphite Composites Made with Cu-Coated and Uncoated Graphite Powders," *Wear*, 253, 2002, pp 699-710.
- [25] Savaskan, T. and Azakli, Z., "An Investigation of Lubricated Friction and Wear Properties of Zn-40Al-2Cu-2Si Alloy in Comparison with SAE 65 Bearing Bronze," *Wear*, 264, 2008, pp 920-928.
- [26] Dhokey, N. B. and Paretkar, R. K., "Study of Wear Mechanisms in Copper-Based SiCp (20% by Volume) Reinforced Composite," *Wear*, 265, 2011, pp 117-133.
- [27] Zhan, Y. and Zhang, G., "The Role of Graphite Particles in the High-Temperature Wear of Copper Hybrid Composites against Steel," *Materials and Design*, 27, 2006, pp 79-84.
- [28] O. I. Ali. "Investigation the parameters Affecting the fabrication of porous metal by p/m". M.S. thesis, Univ. of Babylon, Babil, Iraq, 2017.
- [29] ASTM B-328, "Standard Test Method for Density, Oil Content, and Interconnected Porosity of Sintered Metal Structural Part and Oil - Impregnated Bearing" "ASTM international. 2003.
- [30] Nawal Mohammed Dawood and Enass L Ali, The Effects of Chemical Oxidation on Corrosion Behavior of Ni-Ti Alloy. *IOP Conf. Series: Materials Science and Engineering*, 1094 (2021) 012160 ,pp. 1-10. doi:10.1088/1757-899X/1094/1/012160
- [31] Nawal Mohammed Dawood, Erosion-Corrosion Behavior of Al-20%Ni-Al₂O₃ Metal Matrix Composites by Stir Casting, *Materials Science Forum*, Vol. 1002, 2020, pp 161-174
- [32] Noor Aini Bohari, Shafiquzzaman Siddiquee, Suryani Saallah, Mailin Misson and Sazmal Effendi Arshad, Optimization and Analytical Behavior of Electrochemical Sensors Based on the Modification of Indium Tin Oxide (ITO) Using PANI/MWCNTs/AuNPs for Mercury Detection, *Sensors* 2020, 20, 6502, pp.1-17.
- [33] Yifeng Yao 1 and Yajun Zhou, Effects of Deep Cryogenic Treatment on Wear Resistance and Structure of GB 35CrMoV Steel, Effects of Deep Cryogenic Treatment on Wear Resistance and Structure of GB 35CrMoV Steel, *Metals - Open Access Metallurgy Journal* 8(7):502, June 2018, DOI:10.3390/met8070502.

- [34] Farid A and Syed J A , Microstructure, Mechanical Properties, Electrical Conductivity and Wear Behavior of High Volume TiC Reinforced Cu-Matrix Composites Materials characterization ,2009, 60.327 – 336.
- [35] Haydar Al-Ethari , Ali H. Haleem , Osamah I. Ali , Optimization of Manufacturing Parameters Affecting on Characterization of Porous Sintered Tin-Bronze Alloy, International Journal of Engineering & Technology, 8 (1.5) ,2019, 299-307.
- [36] Nawal Mohammed Dawood , Kadhim F Al-Sultani and Hussein Hatem Jasim, The role of zirconia additions on the microstructure and corrosion behavior of Ni-Cr dental alloys, Mater. Res. Express 8, 2021, 045404,
- [37] Nawal Mohammed Dawood, Abdul Raheem Kadhim AbidAli, Influence of Titanium Additions on the Corrosion Behavior of Cu-Al-Ni Shape Memory Alloys, Materials Science Forum, Vol. 1021, 2021,pp 55-67.
- [38] ABDULRAHEEM KADHIM ABID ALI , NAWAL MOHAMMED DAWOOD, The Effect of Boron Addition on The Microstructure and Corrosion Resistance of Cu-Al-Ni Shape-Memory Alloys Prepared by Powder Technology, IOP Conf. Series: Materials Science and Engineering 987 ,2020, 012028.
- [39] Farid A and Syed J A, Microstructure, Mechanical Properties, Electrical Conductivity and Wear Behavior of High Volume Tic Reinforced Cu-Matrix Composites Materials characterization 60,2009, 327 – 336.
- [40] Bhushan , Principle and Applications of Tribology John Wiley & Sons, Inc., New York, 1999, pp. 343.
- [41] Onat A ,Mechanical and dry sliding wear properties of silicon carbide particulate reinforced aluminium–copper alloy matrix composites produced by direct squeeze casting method Journal of Alloys and Compounds 489, 2010,pp.119-124.
- [42] Mohammad B, Mahmood A and Mehdi A , Cu–Zn–Al₂O₃ nanocomposites: study of microstructure, corrosion, and wear properties International Journal of Minerals, Metallurgy and Materials 24 462.2017.